ATLAS PUB Note
ATL-PHYS-PUB-2022-026
21st July 2022

Study of $t\bar{t}b\bar{b}$ and $t\bar{t}W$ background modelling for $t\bar{t}H$ analyses

The ATLAS Collaboration

This note presents Monte Carlo generator comparisons of the $t\bar{t}b\bar{b}$ and $t\bar{t}W$ processes at particle level. The aim is to compare the modelling of important backgrounds to $t\bar{t}H$ measurements in multi-lepton final states and in the ttH(H→$b\bar{b}$) decay channel and the treatment of the associated theory uncertainties for a combination of the full Run-2 $t\bar{t}H$ results from ATLAS and CMS. As a first step, modelling and theory uncertainties as used in ATLAS are compared in the relevant analysis regions.

Changes made on 18.7.22: changed name of Powheg-box-res to ttbb-Powheg as suggested by theorists to avoid confusion as the resonance-aware algorithm ("-res") is not applied for the ttbb predictions used here. The name is now consistent with the LHC Higgs WG note (https://cds.cern.ch/record/2812088) Corrected pythia version numbers in Tab.1. Added a paragraph on recent developments in ttW theory.

1 Introduction

The search for Higgs boson production in association with a top quark pair ($t\bar{t}H$) in the $H \to b\bar{b}$ [1–4] and in multi-lepton final states [5, 6] analyses is limited by the modelling uncertainties of the main backgrounds, $t\bar{t}b\bar{b}$ and $t\bar{t}W$, respectively. Examples of tree-level diagrams of these processes are shown in Figure 1. A comparison of available Monte Carlo (MC) generators is thus performed to study modelling differences. Comparisons of observables are made at particle level, in a phase space similar to the reference measurements. The goal is to provide input to a discussion on a common strategy for ATLAS and CMS modelling uncertainties in the $t\bar{t}H(b\bar{b})$ and $t\bar{t}H$(multi-lepton) analyses. Comparisons of $t\bar{t}b\bar{b}$ distributions will be presented in Section 2 and of $t\bar{t}W$ distributions in Section 3.

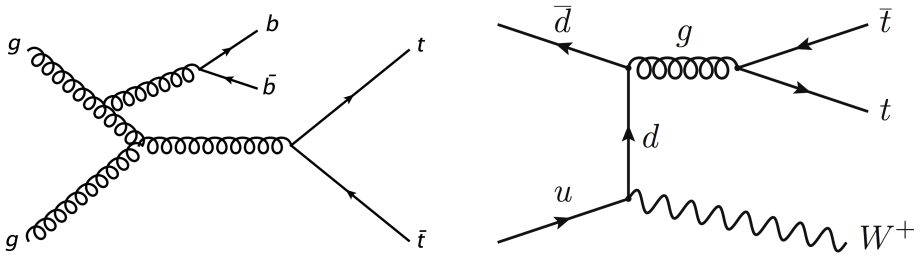

Figure 1: Examples of tree-level Feynman diagrams for $t\bar{t}b\bar{b}$ (left) and $t\bar{t}W$ (right).

2 Comparisons of Monte Carlo predictions for the $t\bar{t}b\bar{b}$ process

In the following section $t\bar{t}b\bar{b}$ background predictions used by ATLAS in published and future analyses of $t\bar{t}H(H \to b\bar{b})$ are compared. Several MC generator implementations where $t\bar{t}b\bar{b}$ matrix elements are calculated at NLO with massive b-quarks[1] using the four-flavour (4FS) scheme [7, 8] are used. The implementation in the Powheg-Box-Res framework [9, 10], referred to as $t\bar{t}b\bar{b}$-Powheg in the following, and matched to Pythia8 [11] for parton shower, hadronization, multi-parton interaction and beam remnant, referred to as parton shower generator for short, is used as nominal prediction in ATLAS physics analyses based on the full Run-2 data set and referred to as PP8 $t\bar{t}b\bar{b}$ in the following.

In order to estimate systematic uncertainties ATLAS considers predictions with different settings of the Powheg internal parameter h_{bzd} which regulates the splitting into the finite and the singular part of the real emission in the NLO calculation. In addition, set-ups of $t\bar{t}b\bar{b}$-Powheg matched to different parton shower generators are considered. Details of these samples are given in [12]. The dependence on the particular choice of generator and the NLO matching algorithm is studied by comparing to predictions of Sherpa 2.2.10 [13–15].

Finally, the uncertainties on the renormalization and factorization scales, μ_{R} and μ_{F}, are estimated by varying them simultaneously in the matrix element (ME) by a factor 0.5 (2) around the nominal value. The dependence on the value of the strong coupling constant, α_s, in the initial and final-state radiation simulation of the parton shower (PS ISR, PS FSR) is estimated by varying them independently also by a factor two up and down, i.e. one scale is changed at a time while keeping the other parameters at their nominal value.

[1] "quarks" refers to both quarks and anti-quarks

The first Run-2 $t\bar{t}H(H \to b\bar{b})$ analysis of ATLAS [1] used a partial data set and based the background predictions on inclusive $t\bar{t}$ production with the matrix element calculated at NLO QCD with Powheg [9, 16–19] employing a 5FS scheme and additional partons including b-quarks produced by the Pythia8 parton shower. The first full Run-2 $t\bar{t}H(H \to b\bar{b})$ analysis [2] changed the nominal generator to PP8 $t\bar{t}b\bar{b}$. However, it used a different set-up compared to the future analyses: the renormalization scale was set to two times the renormalization scale recommended to date by the LHC Higgs WG and the difference between the inclusive $t\bar{t}$ samples was used to derive relative uncertainties which are attached to the nominal PP8 $t\bar{t}b\bar{b}$ sample.

The studies presented here provide comparisons of the PP8 $t\bar{t}b\bar{b}$ prediction with the variations considered to estimate uncertainties for future analyses and comparisons to the predictions used in the first full Run-2 $t\bar{t}H(H \to b\bar{b})$ analyses. All comparisons are performed using stable final state particles in a fiducial phase space similar to the experimental measurements implemented in a dedicated routine in the Rivet analysis toolkit [20].

The section is organised as follows: in Sec. 2.1 describes the samples used for the comparison and the technical set-up of their generation. Section 2.2 describes the observables and the fiducial phase space used for the comparison and finally, Sec. 2.3 displays the resulting comparisons.

2.1 MC generator set-ups

The set-ups used to generate $t\bar{t}b\bar{b}$ predictions with $t\bar{t}b\bar{b}$-Powheg, Powheg, MG5_aMC@NLO and Sherpa are described in the following. The generator configurations and version numbers are summarised in Table 1 and their scale settings are given in Table 2. The systematic uncertainty estimates due to scale variations are summarised in Table 3.

The b-quark mass is set to 4.75 GeV for Sherpa and to 4.95 GeV for all other ATLAS samples. The top quark mass is assumed to be 172.5 GeV. The decay of the top quark is calculated by the corresponding generators (Powheg, Sherpa) respecting the spin correlation. The PDF sets are selected from the NNPDF3.0 family for all samples. The $t\bar{t}b\bar{b}$-Powheg and Powheg samples use EvtGen [21] for simulation of the B-hadron decays.

$t\bar{t}b\bar{b}$-Powheg samples:

Nominal $t\bar{t}b\bar{b}$ predictions are calculated using the Powheg-Box-Res framework at NLO with massive b-quarks [10] with the "4FS NLO as 0118" PDF sets. The Powheg internal parameter h_{bzd} is set to 5. The renormalization scale is set to the geometric average of the transverse mass of top- and b-quarks defined as $m_{\text{T},i} = \sqrt{m_i^2 + p_{\text{T},i}^2}$, where m_i refers to the mass, $p_{\text{T},i}$ to the transverse momentum and i to the top or b-quark. The factorization scale is related to the average of the transverse mass of the outgoing partons in the matrix element calculation, see Table 2. The Pythia8 parameters for parton shower and hadronization modelling are set to the A14 [22] tune. These samples are referred to as PP8 $t\bar{t}b\bar{b}$ samples.

For the h_{bzd} variation, the parameter h_{bzd} is set to 2 in $t\bar{t}b\bar{b}$-Powheg. For the parton shower variations, the set of LHE files which store the results of the matrix element calculation by $t\bar{t}b\bar{b}$-Powheg for the PP8 sample are used and matched to a different parton shower prediction. For the prediction with Pythia8 dipole shower only the treatment of the recoil of the radiated parton in the shower is changed and all other parameters are kept as the A14 tuned values. Another sample is produced where Herwig7 is used with the default tune provided with this generator version.

The $t\bar{t}b\bar{b}$-Powheg samples were calculated using a special option where virtual corrections are switched off and then reweighted with virtual corrections switched on[2].

Sherpa $t\bar{t}b\bar{b}$ samples:

A Sherpa $t\bar{t}b\bar{b}$ sample was generated using Sherpa version 2.2.10 [13–15]. The $t\bar{t}b\bar{b}$ matrix elements were calculated with massive b-quarks at NLO, using the COMIX [23] and Openloops [15] matrix element generators, and merged with the Sherpa parton shower, tuned by the authors [24]. The same renormalization and factorization scales and PDFs are used as for the PP8 $t\bar{t}b\bar{b}$ prediction.

Inclusive $t\bar{t}$ samples:

The inclusive $t\bar{t}$ samples are generated with the Powheg v2 NLO event generator [9, 16–19] and MG5_aMC@NLO+Pythia8 using a five-flavour (5FS) scheme. The renormalization and factorization scales were set to the average transverse mass of the top quark and antiquark.

For the Powheg samples, the h_{damp} parameter[3] was set to the 1.5 times the top quark mass. One sample is generated with the parton shower and hadronization modeled by Pythia8 with the same versions and settings as for the PP8 $t\bar{t}b\bar{b}$ sample above. Another sample is generated using Herwig7 for the parton shower and hadronization. The Powheg $t\bar{t}$ samples are filtered to contain only semi-leptonic and dileptonic $t\bar{t}$ decays with exactly one or two leptons, respectively, within the fiducial volume as defined further below. These samples are referred to as PP8 $t\bar{t}$ and PH7 $t\bar{t}$ samples.

The inclusive MG5_aMC@NLO+Pythia8 $t\bar{t}$ sample uses the same scale settings and the same Pythia8 version as the PP8 $t\bar{t}$ sample and is referred to as aMC+P8 $t\bar{t}$ sample.

[2] steered via "for_reweight 1"

[3] The h_{damp} parameter controls the p_{T} of the first additional emission beyond the leading-order Feynman diagram in the PS and therefore regulates the high-p_{T} emission against which the $t\bar{t}$ system recoils.

Table 1: Configurations used for the event generation of $t\bar{t}b\bar{b}$ processes and the predicted total cross section for events with at least one lepton.

	name	ME	Generator	ME order	Shower	Tune[a]	NNPDF PDF set	h_{damp}	h_{bzd}	$\sigma^{\geq 1\text{lep}}$ [pb]
ATLAS	PP8 $t\bar{t}b\bar{b}$	$t\bar{t}b\bar{b}$	Powheg-Box-Res	NLO	Pythia 8.224	A14	4FS 3.0 NLO as 0118	$H_T/2$	5	18.72
ATLAS	PP8 $t\bar{t}b\bar{b}$ h_{bzd} 2	$t\bar{t}b\bar{b}$	Powheg-Box-Res	NLO	Pythia 8.224	A14	4FS 3.0 NLO as 0118	$H_T/2$	2	18.46
ATLAS	PP8 $t\bar{t}b\bar{b}$ dipole	$t\bar{t}b\bar{b}$	Powheg-Box-Res	NLO	Pythia 8.224	A14, dipoleRecoil[b]	4FS 3.0 NLO as 0118	$H_T/2$	2	18.72
ATLAS	PH7 $t\bar{t}b\bar{b}$	$t\bar{t}b\bar{b}$	Powheg-Box-Res	NLO	Herwig 7.1.6	default	4FS 3.0 NLO as 0118	$H_T/2$	5	18.47
ATLAS	Sherpa $t\bar{t}b\bar{b}$	$t\bar{t}b\bar{b}$	Sherpa 2.2.10	NLO	Sherpa	default	4FS 3.0 NNLO as 0118	—	—	20.24
ATLAS	PP8 $t\bar{t}$	$t\bar{t}$	Powheg v2	NLO	Pythia 8.210	A14	5FS 3.0 NLO	$1.5 \cdot m_{\text{top}}$	5	451.78[c]
ATLAS	PH7 $t\bar{t}$	$t\bar{t}$	Powheg v2	NLO	Herwig 7.13	default	5FS 3.0 NLO	$1.5 \cdot m_{\text{top}}$	5	451.78[c]
ATLAS	aMC+P8 $t\bar{t}$	$t\bar{t}$	MG5_aMC@NLO	NLO	Pythia 8.210	A14	5FS 3.0 NLO	—	—	451.78[c]

[a] "default" refers to the generator's default tune
[b] called by SpaceShower::dipoleRecoil "on"
[c] cross section predicted by NNLO calculation

Table 2: Scale choices used in the event generation of $t\bar{t}b\bar{b}$ and $t\bar{t}$ processes for the different generators.

ME Generator	μ_{R}	μ_{F}
ATLAS Powheg-Box-Res $t\bar{t}b\bar{b}$	$\frac{1}{2}\sqrt[4]{m_{\mathrm{T,t}} \cdot m_{\mathrm{T},\bar{t}} \cdot m_{\mathrm{T,b}} \cdot m_{\mathrm{T},\bar{\mathrm{b}}}}$	$\frac{1}{2}(m_{\mathrm{T,t}} + m_{\mathrm{T},\bar{\mathrm{t}}} + m_{\mathrm{T,b}} + m_{\mathrm{T},\bar{\mathrm{b}}} + m_{\mathrm{T,g}})$
Sherpa 2.2.10	$\frac{1}{2}\sqrt[4]{m_{\mathrm{T,t}} \cdot m_{\mathrm{T},\bar{t}} \cdot m_{\mathrm{T,b}} \cdot m_{\mathrm{T},\bar{\mathrm{b}}}}$	$\frac{1}{2}(m_{\mathrm{T,t}} + m_{\mathrm{T},\bar{\mathrm{t}}} + m_{\mathrm{T,b}} + m_{\mathrm{T},\bar{\mathrm{b}}} + m_{\mathrm{T,g}})$
ATLAS Powheg $t\bar{t}$	$\sqrt{0.5 \cdot (m^2_{\mathrm{T,t}} + m^2_{\mathrm{T},\bar{t}})}$	$\sqrt{0.5 \cdot (m^2_{\mathrm{T,t}} + m^2_{\mathrm{T},\bar{t}})}$
ATLAS aMC $t\bar{t}$	$\sqrt{0.5 \cdot (m^2_{\mathrm{T,t}} + m^2_{\mathrm{T},\bar{t}})}$	$\sqrt{0.5 \cdot (m^2_{\mathrm{T,t}} + m^2_{\mathrm{T},\bar{t}})}$

Table 3: Systematic variations of scales in the matrix element and parton shower codes used for all comparisons presented here.

Variation	
Scale variation ME	$\mu_R \times 0.5\ \mu_F \times 0.5$; $\mu_R \times 2\ \mu_F \times 2$
ISR variation (PS)	$\alpha_s^{ISR} \times 0.5, 2.0$
FSR variation (PS)	$\alpha_s^{FSR} \times 0.5, 2.0$

2.2 Object reconstruction, observables and fiducial volume

The object and event selection applied in this comparison study is defined at particle-level. All objects are defined using stable final state particles with a mean lifetime of $\tau > 3 \times 10^{-11}$ s. Jets are reconstructed from all stable final state particles (but excluding leptons and neutrinos from the top quark decay chain) using the anti-k_t jet algorithm [25, 26] with a radius parameter of $R = 0.4$. Jets which contain at least one ghost-associated [27] B-hadron with transverse momentum (p_T) of $p_T \geq 5$ GeV are defined as b-jets, all other jets are considered "light" jets. The four-momentum of the bare leptons from top quark decay are modified ("dressed") by adding the four-momenta of all radiated photons within a cone of size $\Delta R = 0.1$. All objects are considered within pseudo-rapidity $|\eta| \leq 2.5$ and with $p_T > 27$ GeV for leptons and $p_T > 25$ GeV for jets and b-jets.

Leptons are removed if they are separated from a jet by less than $\Delta R = 0.4$, where $\Delta R = \sqrt{(\Delta\eta)^2 + (\Delta\phi)^2}$. Events are selected with at least four b-jets, and further separated into two analysis regions: events with exactly one lepton and at least six jets (single lepton channel) and events with exactly two leptons and at least four jets (dilepton channel).

A set of observables relevant for the $t\bar{t}H(H \to b\bar{b})$ analysis is studied within this fiducial phase space. All observables are studied for both the single lepton and the dilepton channel, however only the variables listed in Table 4 are shown in the following figures, as no significant qualitative difference is observed between the different top quark decay channels.

Table 4: The list of observables used for the comparison of the generators for the $t\bar{t}b\bar{b}$ process.

Variable	Description	Channel
$\Delta R_{bb}^{\min\Delta R}$	ΔR of the two b-jets in the event which are closest in ΔR	dilepton
$m_{bb}^{\min\Delta R}$	Invariant mass of the two b-jets closest in ΔR	dilepton
N_{jets}	Number of jets in the event (all jet flavours)	dilepton
Light jet p_T	Transverse momentum of the light jets in the event	dilepton
$N_{b\text{-jets}}$	Number of b-jets in the event	single lepton
H_T^{jets}	Scalar sum of p_T of jets in the event (all jet flavours)	single lepton
Leading b-jet p_T	p_T of b-jet with largest p_T in the event	single lepton
Fourth b-jet p_T	p_T of b-jet with fourth largest p_T in the event	single lepton

2.3 Results

Three sets of generator predictions are compared on the observables given in Table 4 as follows. All comparisons are performed with respect to the PP8 $t\bar{t}b\bar{b}$ sample. The PP8 $t\bar{t}b\bar{b}$ sample and the alternative predictions are normalised to an integral of 1, after all selections and in each histogram individually for a shape-only comparison. The scale uncertainty variations on PP8 $t\bar{t}b\bar{b}$ are derived as listed in Table 3 and the differences are added in quadrature to form the shaded area displayed in the figures.

Figure 2 shows the nominal $t\bar{t}b\bar{b}$ predictions compared to the nominal predictions used in the early Run-2 analyses. Significant differences between the PP8 $t\bar{t}b\bar{b}$ predictions and the PP8 $t\bar{t}$ predictions are observed in $\Delta R_{b\bar{b}}^{\mathrm{min}\Delta R}$, the jet multiplicity and in the number of events with more than four b-jets.

In Figure 3, the nominal PP8 $t\bar{t}b\bar{b}$ prediction is compared to all generator variations potentially considered for modelling uncertainty for the ATLAS $t\bar{t}H(H \to b\bar{b})$ analysis, i.e. variations in Powheg-Box-Res and Pythia8 parameter settings as well as Sherpa as alternative generator. As already discussed in [12], the parameter h_{bzd} has only a minor influence on the observables. Interestingly, predictions of Powheg-Box-Res matched to Pythia8 with dipole shower and matched to Herwig parton shower are similar and both show a significant decrease with respect to the nominal PP8 $t\bar{t}b\bar{b}$ in the jet multiplicity and H_{T}. Sherpa differs up to 10–20 % in all distributions mostly towards the edges of the phase space. Differences are in jet kinematics and in particular increasing differences towards high values are observed for $\Delta R_{b\bar{b}}^{\mathrm{min}\Delta R} > 1.5$.

Finally, Figure 4 shows the distributions used to estimate the systematic modelling uncertainties of the first full Run-2 analysis by ATLAS [1]. The uncertainty on the $t\bar{t}b\bar{b}$ PP8 prediction is estimated by assigning the relative difference between PP8 $t\bar{t}$ and alternative $t\bar{t}$ predictions listed in Table 1 to the $t\bar{t}b\bar{b}$ prediction.

2.4 Conclusions

Comparisons of generator predictions used by ATLAS in a typical phase space of the $t\bar{t}H(H \to b\bar{b})$ measurement were presented. Two sets are used for comparison: the generators used in the most recent published analyses involving $t\bar{t}$ inclusive predictions based on 5FS scheme to estimate uncertainties and the set of generators in the future effort using $t\bar{t}b\bar{b}$ calculations at NLO based on the 4FS scheme.

The difference between the predictions exceeds the uncertainties from the scale variations both for the uncertainties considered in the published $t\bar{t}H(H \to b\bar{b})$ analysis and for the future analyses. Smaller uncertainties due to the choice of parton shower and NLO generator are observed when estimating them based on $t\bar{t}b\bar{b}$ ME predictions compared to the previously used $t\bar{t}$ ME matched predictions.
These distributions will be used in a future comparison of theory uncertainties between ATLAS and CMS.

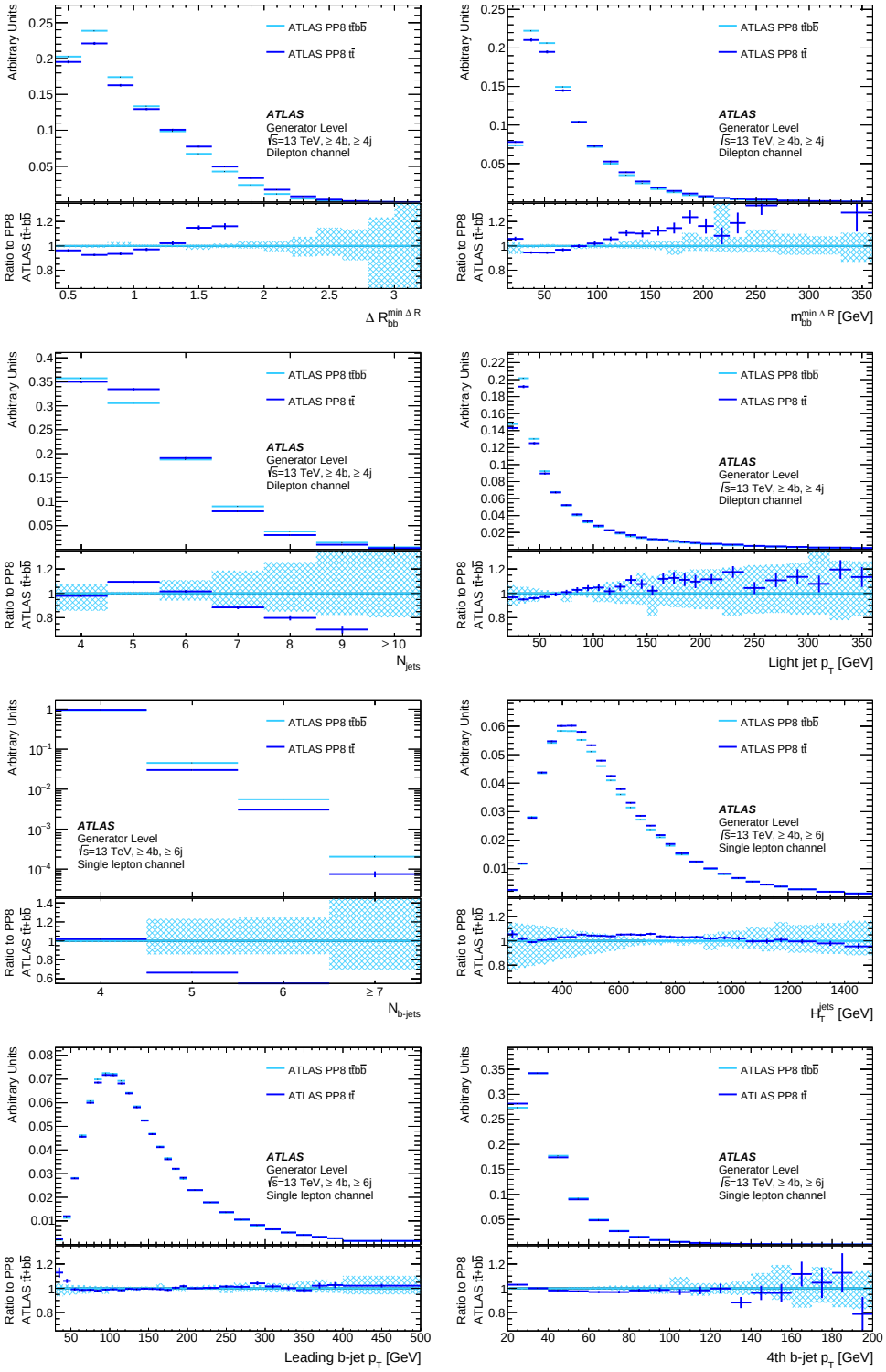

Figure 2: Comparison of PP8 predictions for $t\bar{t}b\bar{b}$ and $t\bar{t}$ with the described settings using the observables defined in Table 4 in the fiducial analysis phase space. All predictions are normalised to 1. The error bands contain the scale variations (matrix element and parton shower) for the PP8 $t\bar{t}b\bar{b}$ (blue) sample. Statistical uncertainties are indicated by vertical lines. The ratio shows the different curves divided by the PP8 $t\bar{t}b\bar{b}$ prediction.

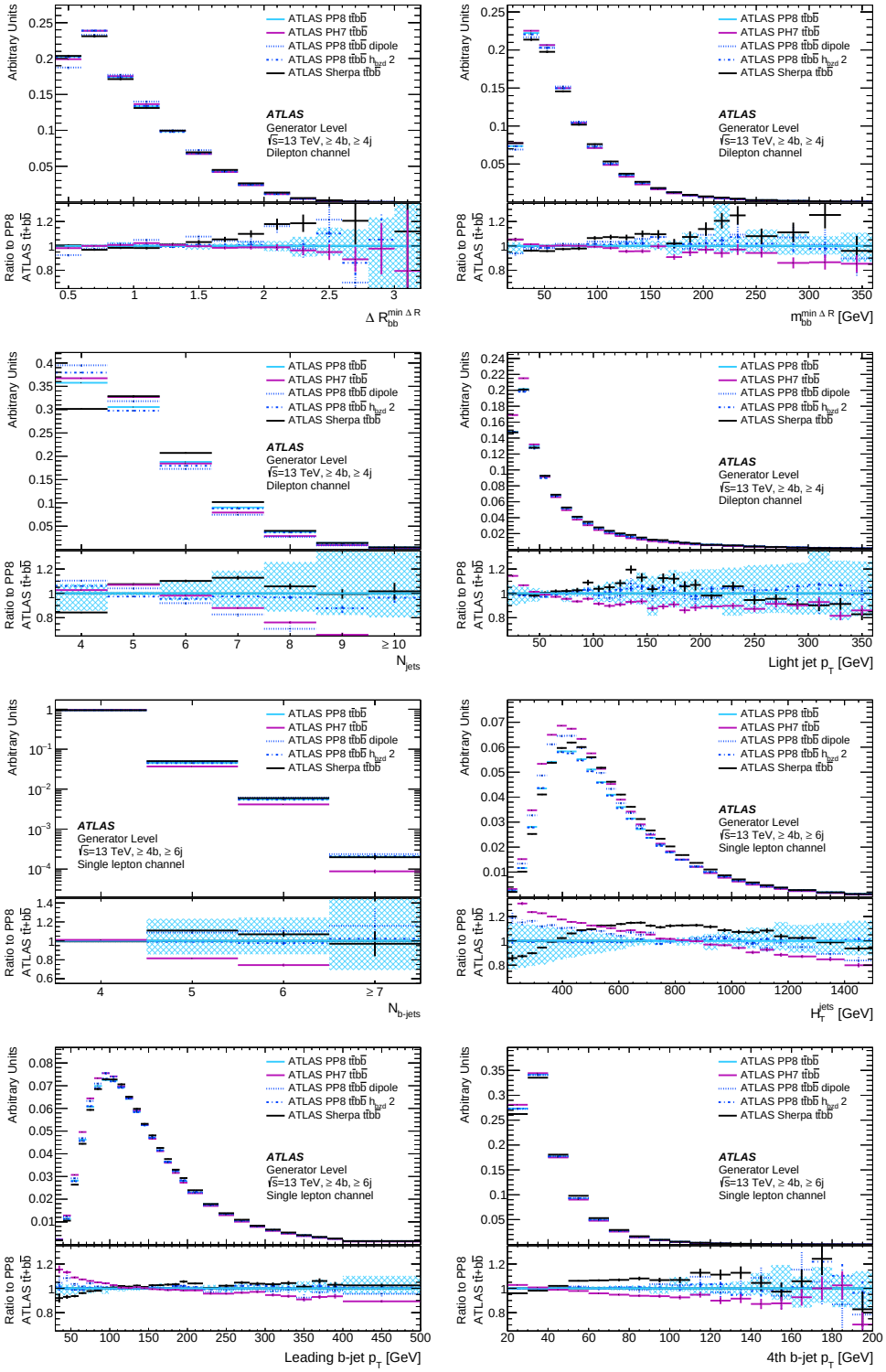

Figure 3: Comparison of PP8 predictions for $t\bar{t}b\bar{b}$ with different matching and parton shower settings and SHERPA. All distributions are normalised to 1. The ratio shows the different curves divided by PP8 $t\bar{t}b\bar{b}$. The error band contains the scale variations (matrix element and parton shower) as defined in the text for the PP8 $t\bar{t}b\bar{b}$ sample. Statistical uncertainties are indicated by vertical lines.

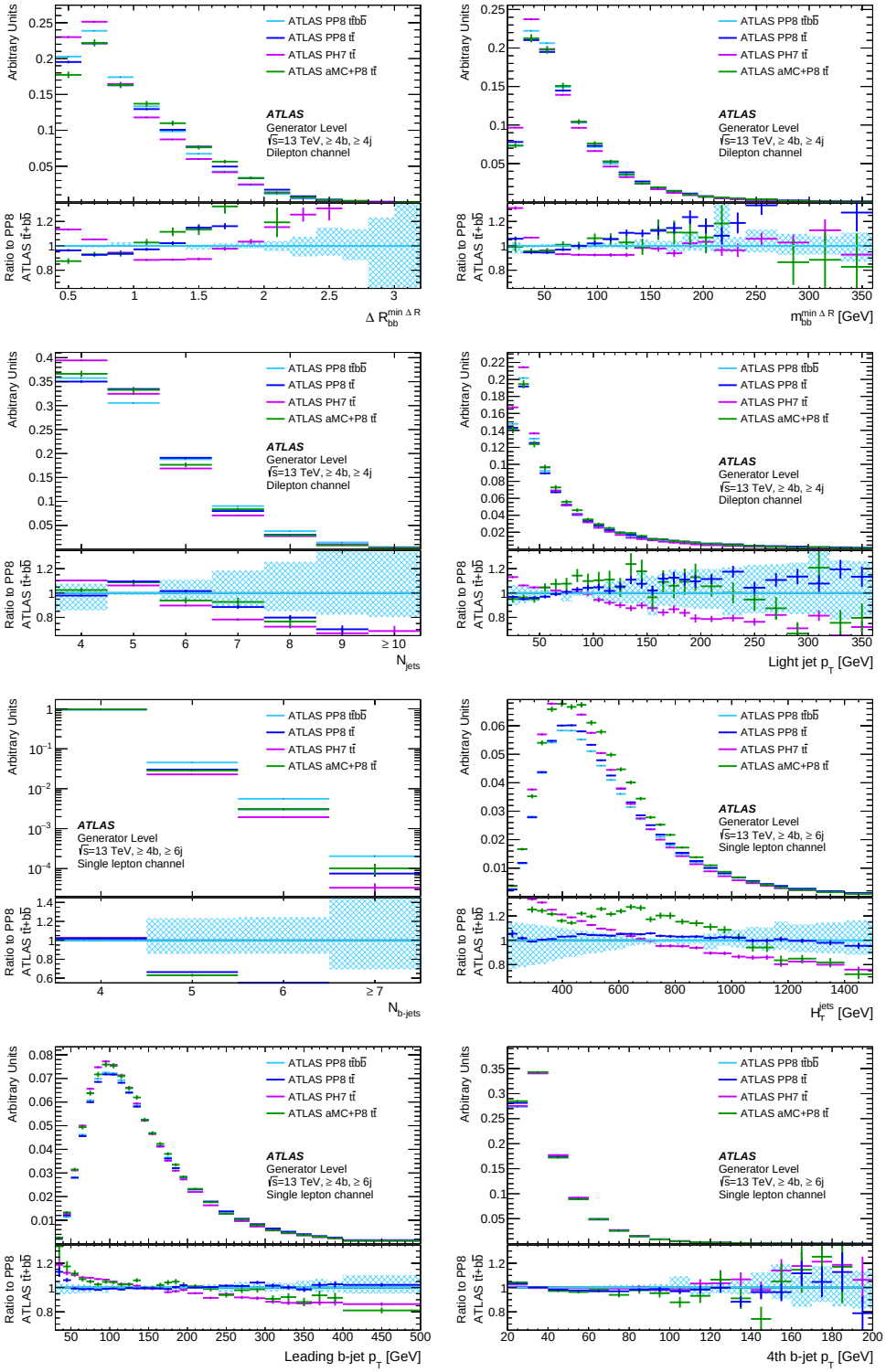

Figure 4: Comparison of predictions used for the systematic uncertainties of the first full Run-2 analysis by ATLAS [1]. All distributions are normalised to 1. The ratio shows the different curves divided by PP8 $t\bar{t}b\bar{b}$. The blue error band contains the scale variations (matrix element and parton shower) as defined in the text for the PP8 $t\bar{t}b\bar{b}$ sample. Statistical uncertainties are indicated by vertical lines.

3 Comparison of MC predictions for the $t\bar{t}W$ process

The CMS [6] and ATLAS experiments [5] measured the $t\bar{t}H$ production cross section in multi-lepton final states which are primarily sensitive to the decays of H$\rightarrow WW^*$, H$\rightarrow \tau\tau$ and H$\rightarrow ZZ^*$. The dominant background in these measurements stems from $t\bar{t}W$ production. These measurements along with the recent CMS measurement of $t\bar{t}W$ production [28] show some tension with the SM predictions. In order to describe this background, different theoretical predictions are used for the future and published measurements by ATLAS and will be described in the following.

In recent times there have been significant theoretical developments in $t\bar{t}W$ modelling despite the challenges associated with calculations of $t\bar{t}W$ with higher order corrections in the QCD, α_s, and EWK, α, couplings. Even at LO in α_s, complications arise because $t\bar{t}W$ is a qq-initiated process in which the radiation of the W-boson from one of the initial state quarks polarises the incoming quark, making spin correlations all the more important [29]. Initial calculations of $t\bar{t}W$ production at next-to-leading order (NLO) in QCD at fixed order [30] and later matched to a parton shower [31–33] were later augmented with NLO EWK corrections (of order $\alpha^2\alpha_s^2$) [34] to provide the higher order cross sections used across the LHC programme for a number of years [35]. Since then there has been significant theoretical progress in calculating more complex and precise predictions. Higher order QCD corrections including $t\bar{t}W$ production with additional partons open gluon-initiated production modes with significant contributions to the total cross section. Recent studies show that these contributions also have large next-to-leading order (NLO) corrections [36] and that $t\bar{t}W\,jj$ can be large [37], both of which require NLO-merged calculations [38] for such effects to be properly included. Furthermore, beyond the traditionally "leading" NLO EWK corrections (of order $\alpha^2\alpha_s^2$) there are even larger contributions from traditionally "sub-leading" NLO corrections (of order $\alpha^3\alpha_s$) [33, 39, 40] due to the existence of tW scattering contributions embedded in to the $t\bar{t}W\,j$ process. Calculations at NLO in QCD accounting for next-to-next-to-leading logarithmic effects (NNLL) are also available [41] as well as recent predictions at NLO+NNLL in QCD also with NLO EWK corrections [42, 43]. Full off-shell calculations at NLO in QCD [44–46] are also now available and more recently the NLO EWK corrections have also been incorporated [47] into these calculations, along with the development of procedures to apply the off-shell corrections to NLO+PS setups [48].

For future analyses, updated MC models will be used and the estimate of systematic uncertainty is under development. The latest setups tested by ATLAS are documented in the following. The use of other theoretical developments, already outlined, will also be considered in future but are beyond the scope of this document.

3.1 MC generator set-ups

The nominal sample for inclusive $t\bar{t}W$ production was generated using the Sherpa 2.2.10 [13, 49] generator with the NNPDF3.0 NLO PDF set. The matrix element (ME) was calculated for up to one additional parton at NLO and up to two partons at LO using Comix [23] and OpenLoops [15], and merged with the Sherpa parton shower [24] using the MEPs@Nlo prescription [50] with a merging scale of 30 GeV. The choice of renormalization and factorization scales is $\mu_R = \mu_F = H_T/2$, where H_T is defined as the scalar sum of the transverse masses $\sqrt{p_T^2 + m^2}$ of all final state particles. Detailed information of the Sherpa sample is listed in Table 5. Systematic uncertainties due to missing higher-order QCD corrections are estimated in the nominal sample by varying the factorization and renormalization scales together with α_s in the parton shower by a factor of 0.5 (2.0) with respect to the central value.

In addition to this nominal prediction at NLO in the strong coupling a separate sample is produced which contains also higher order corrections relating to electroweak (EW) contributions. These are added in two ways. First, through event-by-event correction factors of the order α^3 and $\alpha^2\alpha_s^2$ where α (α_s) refers to the EW (QCD) coupling constant. Secondly, sub-leading EW corrections at order $\alpha^3\alpha_s$ [40] are introduced via the addition of an independent Sherpa 2.2.10 sample produced at LO in QCD for this final state. This sample is marked as "QCD+EW" in the following.

Uncertainties associated with the modelling of additional QCD radiation have been estimated by comparing the nominal $t\bar{t}W$ prediction with that of an alternative sample that was generated at NLO with the MadGraph5_aMC@NLO 2.3.3 [51] generator using the same scale choice as for the nominal sample and PDF set NNPDF3.0NLO, and interfaced to Pythia 8.210 [11] in combination with the A14 tune [22].

A $t\bar{t}W$ prediction was produced using the MadGraph5_aMC@NLO 2.9.3 program to generate $t\bar{t}W$ production with up to one additional parton in the final state at NLO accuracy in the strong coupling. The renormalization and factorization scales are the same as in the nominal sample. The showering and subsequent hadronization is performed using Pythia 8.245[11] with the A14 tune [22]. The different jet multiplicities are merged using the FxFx NLO matrix-element and parton-shower merging prescription [52], see detailed description in [53].

The configurations of the samples are summarised in Table 5.

3.2 Object reconstruction, fiducial volume and observables

Object and event selection is defined at particle-level that closely matches the detector-level described in reference [5] (ATLAS) and [6] (CMS). Jets are reconstructed from all stable final state particles with a mean lifetime of $\tau > 3 \times 10^{-11}$ s (but excluding leptons and neutrinos from the top quark decay chain), using the anti-k_t algorithm with a radius parameter of $R = 0.4$. Jets are required to satisfy p_{T} >25 GeV and $|\eta|$ <2.5. Jets that are matched to a b-hadron[4] by ghost matching [27] are referred to as b-jets. Electrons and muons, referred to as light leptons ℓ, are required to be separated from selected jets by $\Delta R > 0.4$ and are otherwise removed. Hadronically decaying τ leptons are required to satisfy p_{T} >25 GeV and $|\eta|$<2.5. Events are selected with exactly two light leptons. The four-momentum of the bare leptons from top quark decay are modified ("dressed") by adding the four-momenta of all radiated photons within a cone of size $\Delta R = 0.1$. Leptons are required to have $|\eta|$<2.5 and p_{T} >25(20) GeV for leading ℓ_0 (subleading ℓ_1) lepton (p_{T} ordered). Leptons are required to have same charge, targeting the semi-leptonic $\mathrm{t\bar{t}}$ decay and leptonic W decay.

Events with at least 3 jets and at least one of them being a b-jet are considered in the fiducial volume. The object definition and event selection is summarised in Tables 6 and 7. These are then split into five regions, categorized by the number of jets of any flavour (three or ≥4), $N_{b-\mathrm{jets}}$ (one or ≥2) as well as the presence of hadronically decaying τ lepton, as summarised in Table 8.

The definitions of the regions are motivated by the $t\bar{t}H$ Multilepton analysis strategy. Regions 1 and 2 corresponds to the signal regions[5] and Regions 3 and 4 are used as control regions in the 2ℓ same-sign 0-τ_{had} $t\bar{t}H$ channel. Definition of Region 5 is closely followed[6] by the selections in the 2ℓ same-sign 1-τ_{had} $t\bar{t}H$ channel.

The list of variables for the comparison of the $t\bar{t}W$ generators presented in this note are summarised in Table 9.

[4] no p_{T} cut is applied
[5] slightly different then in ref. [5], in order to define a common selection with the CMS Collaboration.
[6] requirement on jet multiplicity is relaxed.

Table 5: The configurations used for the event generation of the $t\bar{t}W$ processes. Scale settings given in terms of $H_{\mathrm{T}} = \sum_{i=0}^{i=N} \sqrt{p_{T,i}^2 + m_i^2}$, where N = number of final state particles.

Label	ATLAS Sherpa 2.2.10	ATLAS Sherpa 2.2.10 QCD+EW	ATLAS aMC@NLO FxFx	ATLAS aMC@NLO
Process	$t\bar{t}W$ inclusive	$t\bar{t}W$ inclusive	$t\bar{t}W$ inclusive	$t\bar{t}W$ inclusive
Generator	Sherpa 2.2.10[13]	Sherpa 2.2.10[13]	MG5_aMcAtNlo v2.9.3[54]	MG5_aMcAtNlo v2.3.3[51]
order of QCD ME	0,1@NLO+2@LO	0,1@NLO+2@LO	0,1@NLO	NLO
ME Scale	$\mu_{\mathrm{R}} = \mu_{\mathrm{F}} = H_{\mathrm{T}}/2$	$\mu_{\mathrm{R}} = \mu_{\mathrm{F}} = H_{\mathrm{T}}/2$	$\mu_{\mathrm{R}} = \mu_{\mathrm{F}} = H_{\mathrm{T}}/2$	$\mu_{\mathrm{R}} = \mu_{\mathrm{F}} = H_{\mathrm{T}}/2$
order of EW corrections	-	α^3, $\alpha^2\alpha_s^2$, $\alpha^3\alpha_s$	-	-
Parton Shower	Sherpa 2.2.10	Sherpa 2.2.10	Pythia 8.245[11]	Pythia 8.210[11]
Merging Scheme	MEPs@NLO[50]	MEPs@NLO[50]	FxFx[52]	-
Merging Scale	30 GeV	30 GeV	30 GeV	-
PDF	NNPDF3.0 NNLO[55]	NNPDF3.0 NNLO	NNPDF3.0 NLO	NNPDF3.0 NLO
Tune	Sherpa default	Sherpa default	A14[22]	A14[22]
σ_{tot} [a]	597.0 fb	614.7 fb	613 fb	548 fb

[a] σ_{tot}=600.8 fb from YR4 is used for all samples in the generator comparisons in section 3.3.2

Table 6: The object reconstruction used in the Rivet analysis of the $t\bar{t}W$ processes.

Object reconstruction and selection
Jets: build from stable final state particles with anti-k$_t$ algorithm with radius R = 0.4 the prompt "dressed" leptons and neutrinos are vetoed from jet b-jets: Jets ghost matched to B-hadrons with $p_{\mathrm{T}} > 5$ GeV Jets and b-Jets: $p_{\mathrm{T}} > 25$ GeV and $\|\eta\| < 2.5$
light leptons (electrons and muons) dressed with photons within $\Delta R < 0.1$ Overlap removal: remove light lepton if $\Delta R(jet, lepton) < 0.4$ leptons: $\|\eta\| < 2.5$ and $p_{\mathrm{T}} > 25(20)$ GeV for leading (subleading) lepton hadronicaly decaying τ leptons (before decay): $p_{\mathrm{T}} > 25$ GeV and $\|\eta\| < 2.5$

Table 7: The event selection used in the Rivet analysis for the $t\bar{t}W$ processes. N_{jets} refers to all jets independent of jet flavour, i.e. b-jets are included.

Event selection for 2ℓSS
exactly 2 leptons with same charge
$N_{\mathrm{jets}} \geq 3$
$N_{b-\mathrm{jets}} \geq 1$

Table 8: The region definitions used in the Rivet analysis for the $t\bar{t}W$ processes.

Region	**Selection**
1	$N_{b-\mathrm{jets}} = 1$, $N_{\mathrm{jets}} \geq 4$, 0-τ_{had}
2	$N_{b-\mathrm{jets}} \geq 2$, $N_{\mathrm{jets}} \geq 4$, 0-τ_{had}
3	$N_{b-\mathrm{jets}} = 1$, $N_{\mathrm{jets}} = 3$, 0-τ_{had}
4	$N_{b-\mathrm{jets}} \geq 2$, $N_{\mathrm{jets}} = 3$, 0-τ_{had}
5	$N_{b-\mathrm{jets}} \geq 1$, $N_{\mathrm{jets}} \geq 3$, 1-τ_{had}

Table 9: The list of the validation variables for the comparison of the $t\bar{t}W$ generators. The leptons ℓ and b-jets are ordered in p_{T}- leading correspond to highest p_{T}.

Variable	Description	Regions
N_{jets}	Jet multiplicity	1,2,5
N_{b-jets}	Number of b-jets	1,2,5
$H_{\mathrm{T}}^{\mathrm{jets}}$	Scalar sum of transverse momentum of all jets in the event	1,2,3,4
p_{T}^{b0}	Leading b-jet transverse momentum	1,2
$p_T^{\ell 0}$	Leading lepton transverse momentum	1,2,5
$\Delta R_{\ell 0\mathrm{jets}}$	Minimum angular separation between the leading lepton and the nearest jet	1,2
$\Delta R_{\ell 0 \ell 1}$	Angular distance between the two leptons	1,2,5
$max\|\eta_\ell\|$	Value of the highest lepton's pseudorapidity in the event	1,2

3.3 Results

The samples described in Table 5 are compared in the following. The ratio plots show the ratios of the all MC samples with respect to SHERPA, the shaded band represents scale variations. The same set of distributions are presented twice with different focus: in Sect. 3.3.1 shapes are compared and in Sect. 3.3.2 acceptance effects are studied.

3.3.1 Shape comparison

In the following shape agreement between nominal and alternative generators will be presented, i.e. the distributions are normalised to the integral.

The modelling of jet kinematics are presented on Figure 5 for the high (Regions 1 and 2) and low (Regions 3 and 4) jet multiplicities. Significant differences between SHERPA and MG5_AMC@NLO+Pythia8 are observed which are not present for MG5_AMC@NLO+Pythia8 FxFx.

The lepton kinematics distributions are shown on Figure 7 representing Region 2. Overall, good agreement between all predictions is observed.

The distributions of the angular distance between the two leptons and the maximum of lepton's pseudorapidity separation between the leptons are presented in Figure 8 for Region 1 on the right and Region 2 on the left. Good agreement of the distributions is observed except for MG5_AMC@NLO+Pythia8.

Distributions of the jet multiplicity, number of b-jets, the leading lepton transverse momentum and the angular distance between the two leptons $\Delta R_{\ell 0 \ell 1}$ for the Region 5 with $N_{\tau_{\text{had}}} = 1$ selection are presented in Figure 9. In contrast to all other comparisons, the jet multiplicity prediction of MG5_AMC@NLO+Pythia8 with FxFX differs most from the other predictions in this region.

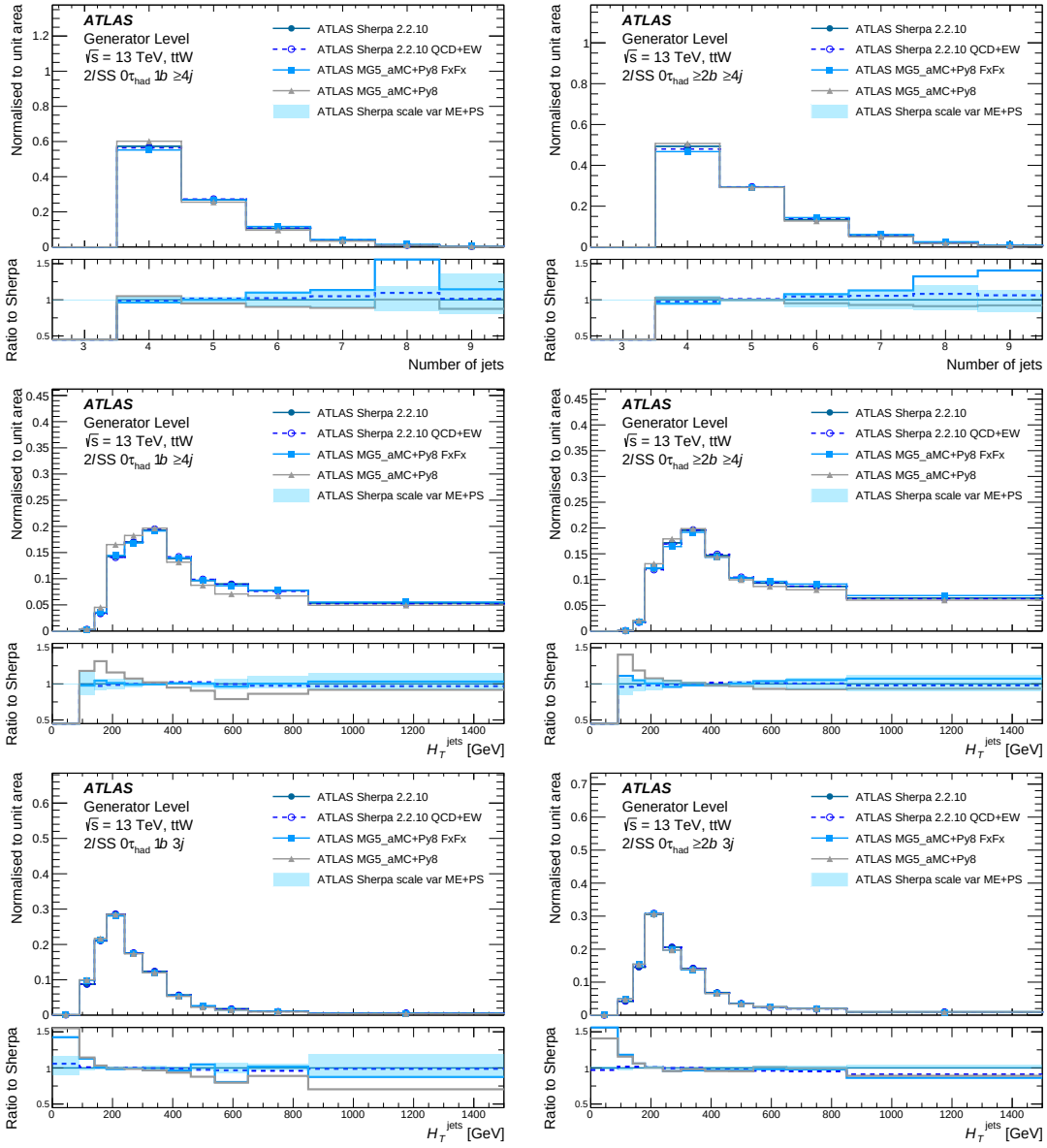

Figure 5: Distribution of the jet multiplicities (top) and the scalar sum of jets transverse momentum, $H_{\mathrm{T}}^{\mathrm{jets}}$ (middle), for the Region 1 with $N_{b-\mathrm{jets}}$ =1 (left) and Region 2 with $N_{b-\mathrm{jets}}$ ≥2 (right) selection requiring four and more jets, and for the Region 3 $N_{b-\mathrm{jets}}$ = 1 (bottom, left) and Region 4 with $N_{b-\mathrm{jets}}$ ≥2 (bottom, right) selection requiring exactly three jets.

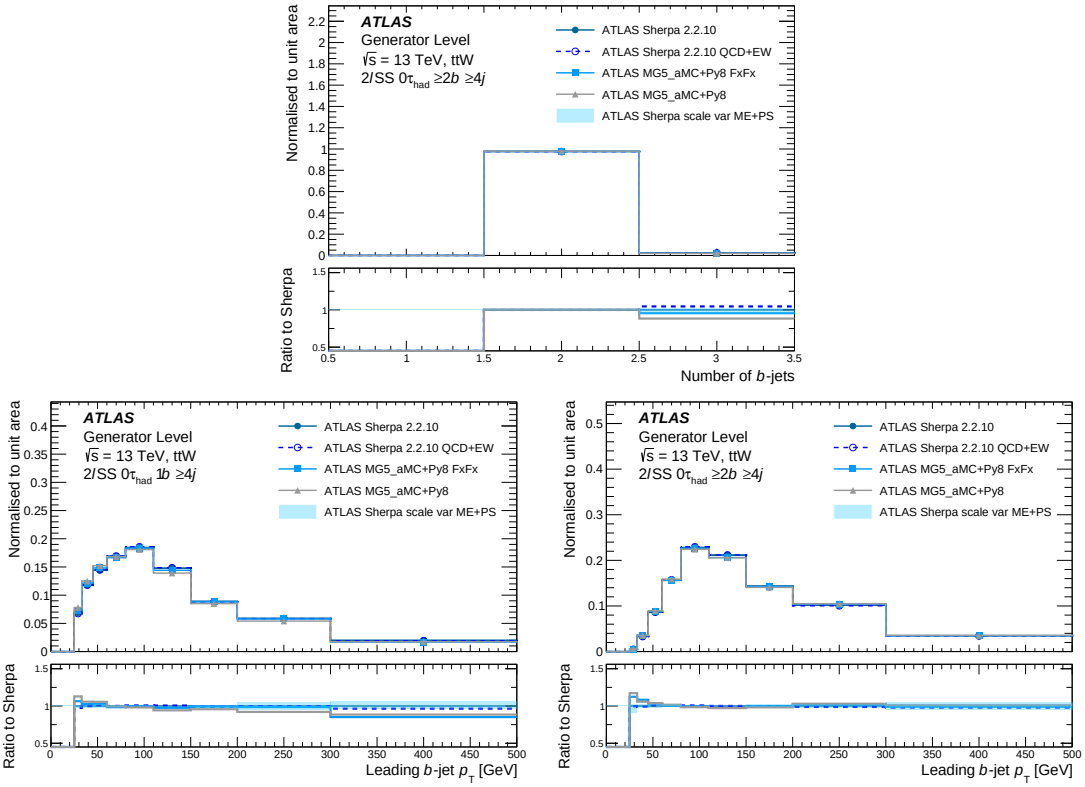

Figure 6: Distribution of the b-jet multiplicities (top) and the leading b-jet transverse momentum (bottom), for the Region 1 with $N_{b-\text{jets}}$=1 (left) and Region 2 with $N_{b-\text{jets}} \geq 2$ (right) selection requiring four and more jets.

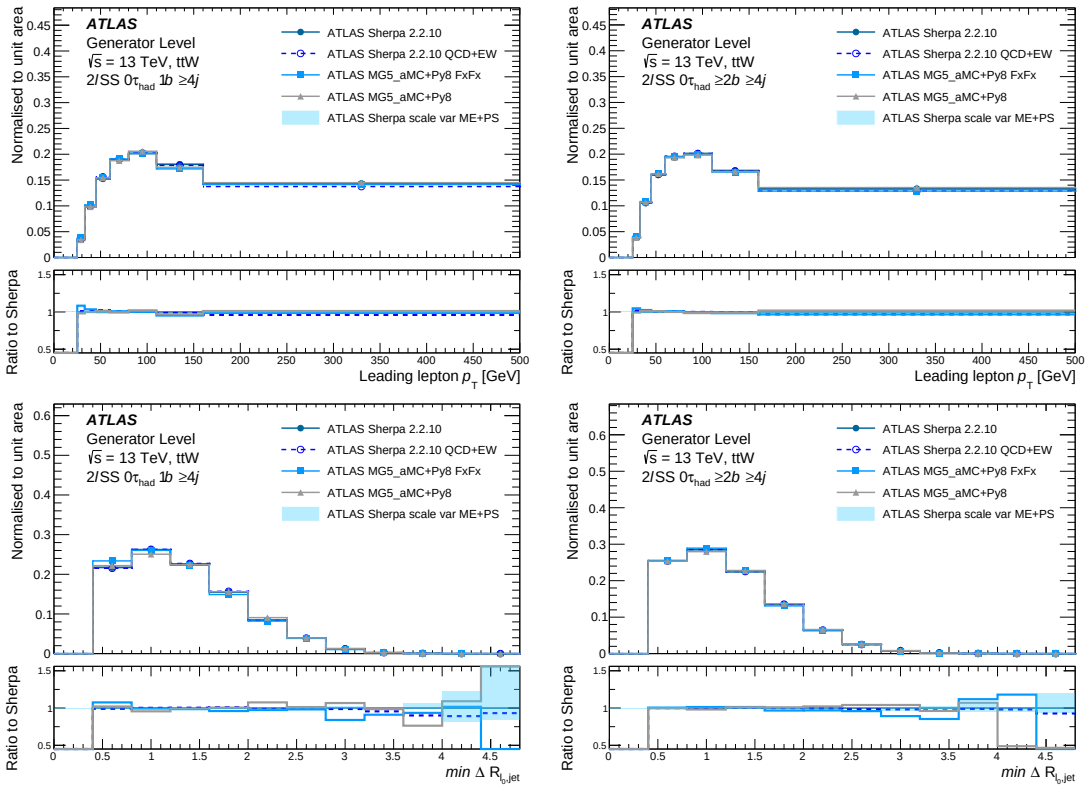

Figure 7: Distribution of the leading lepton transverse momentum (top) and the minimum angular separation between the leading lepton and the nearest jet (bottom), for the Region 1 with $N_{b-\text{jets}}$=1(left) and Region 2 with $N_{b-\text{jets}}$ ≥2(right) selection requiring four and more jets.

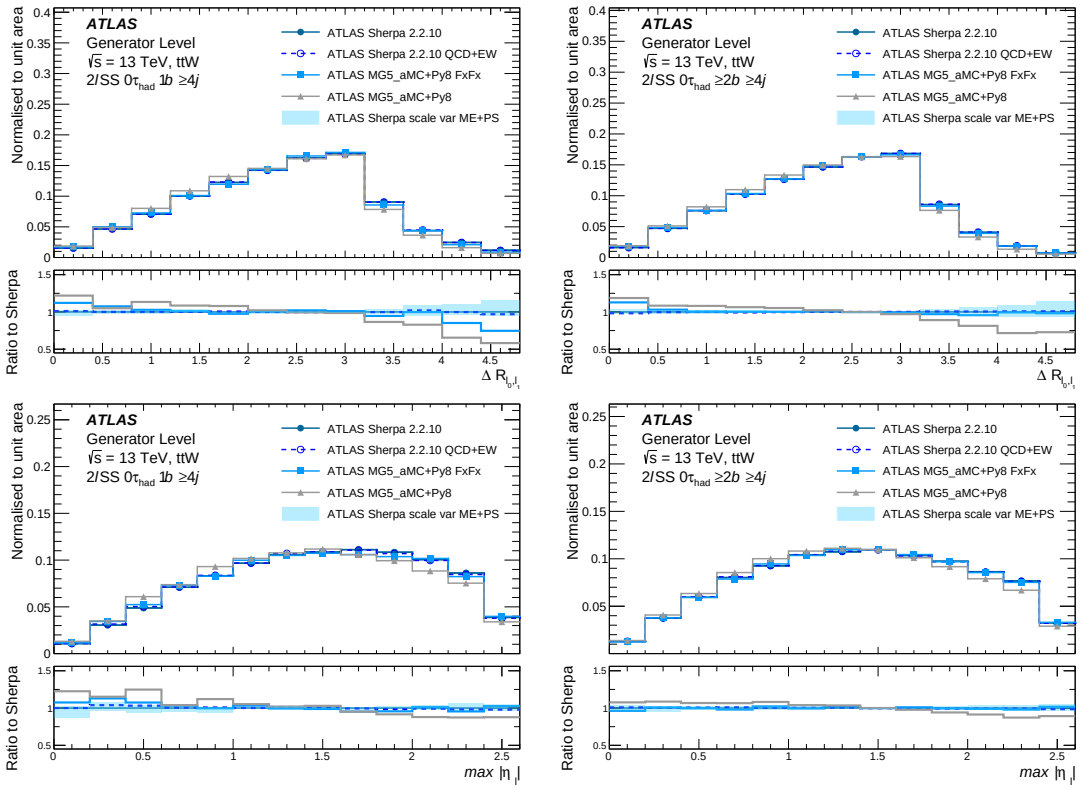

Figure 8: Distribution of the angular distance between the two leptons (top), maximum between lepton $|\eta_{\ell 0}|$ and $|\eta_{\ell 1}|$(bottom) , for the Region 1 with $N_{b-\text{jets}}$=1 (left) and Region 2 with $N_{b-\text{jets}}$ ≥2(right) selection requiring four and more jets.

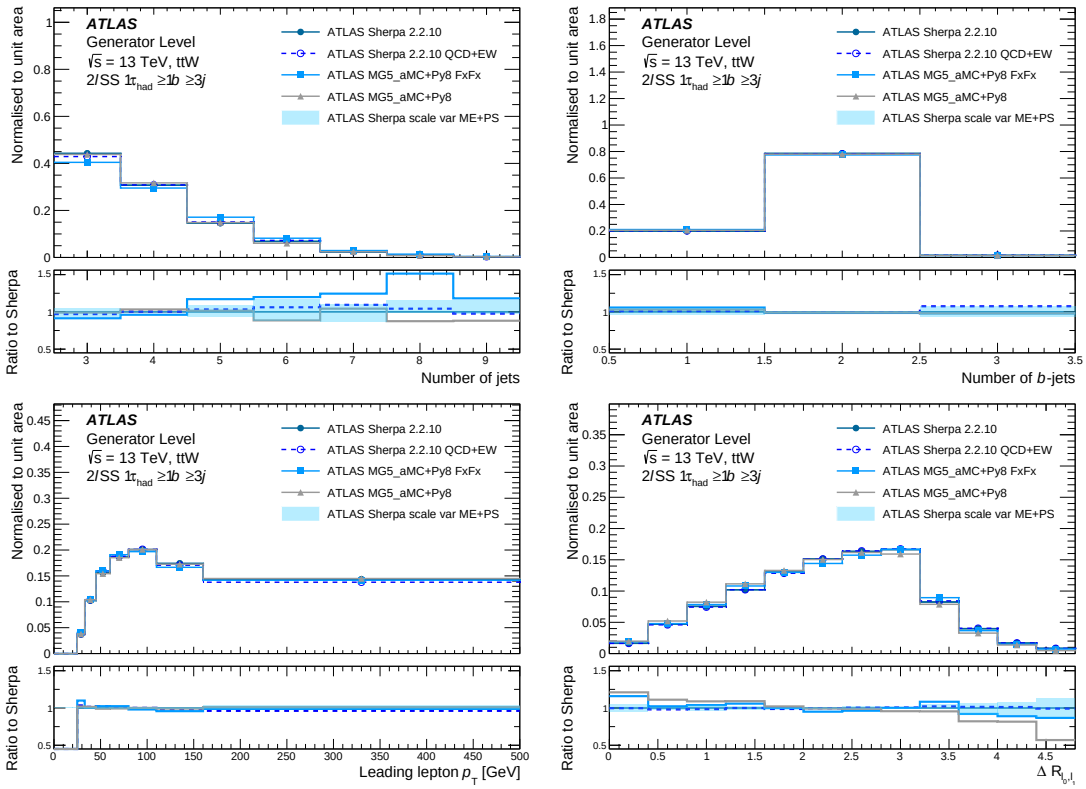

Figure 9: Distribution of the the jet multiplicity, number of b-jets, the leading lepton transverse momentum and the angular distance between the two leptons $\Delta R_{\ell\ell}$ for the Region 5 with $1\tau_{had}$ selection.

3.3.2 Comparisons of predictions including acceptance effects

In the following section a comparison of the generators will be given in the fiducial phase space, i.e. the predicted distributions include acceptance effects. For this comparison, all distributions without EW corrections are normalised to match the total cross section value of σ_{tot}^{YR4} =600.8 fb as given in the Yellow Report 4 [35] for predictions without EW corrections. The distributions of Sherpa QCD+EW which are normalised to their generator cross section of 614.7 fb. The same set of distribution discussed in Section 3.3.1 are presented. In all distribution, a significant increase of scale uncertainties is observed, reaching up to 50% at high jet multiplicity. The observables related to jet multiplicity and H_{T} show similar trends as in the shape comparisons, see Figure 10. Only the discrepancy of the jet multiplicity prediction in MG5_aMC@NLO+Pythia8 FxFx is significantly enhanced.

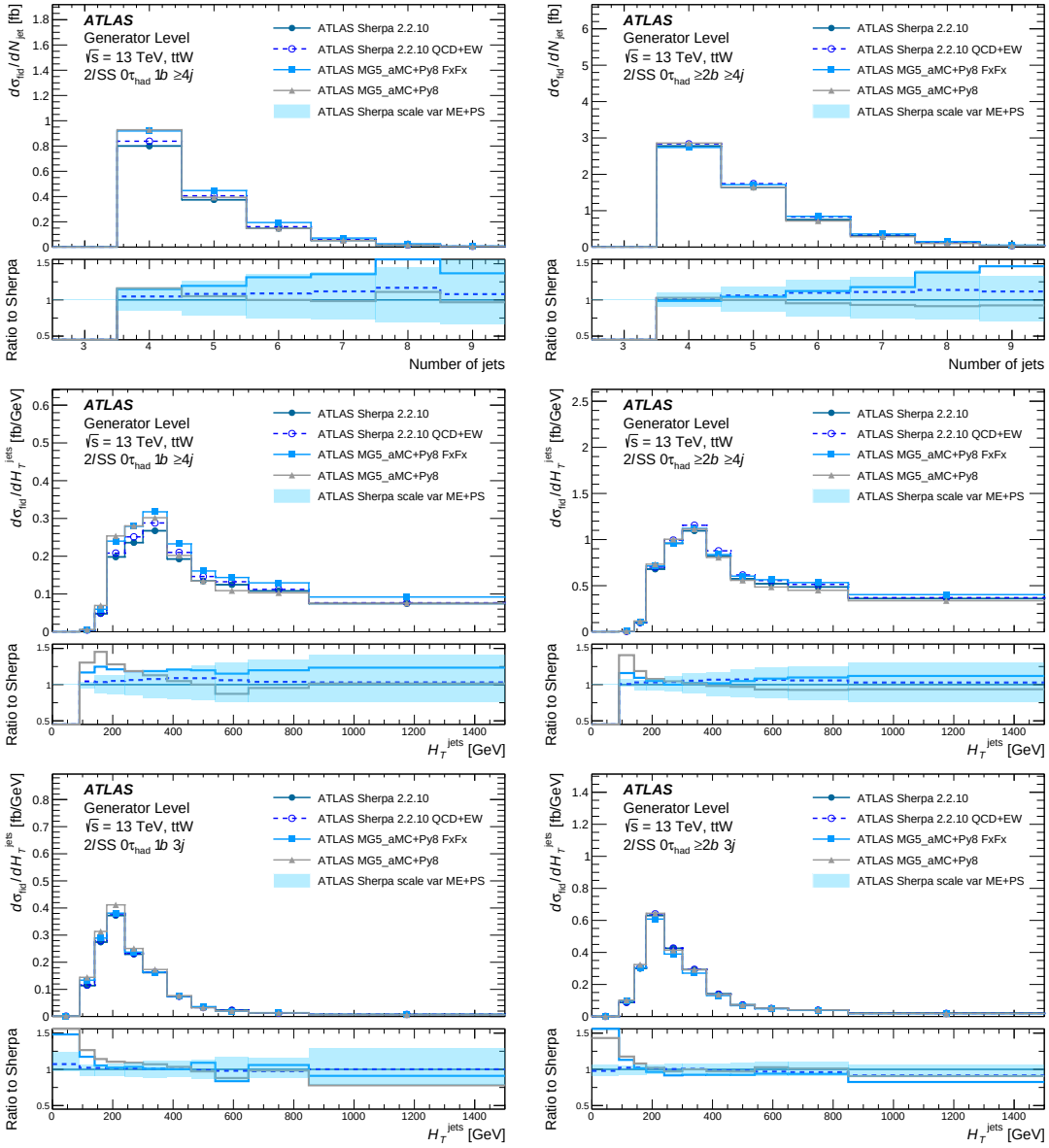

Figure 10: Distribution of the jet multiplicities (top) and the scalar sum of jets transverse momentum, $H_{\mathrm{T}}^{\mathrm{jets}}$ (middle), for the Region 1 with $N_{b-\mathrm{jets}}$=1 (middle, left) and Region 2 with $N_{b-\mathrm{jets}}$ ≥2 (middle, right) selection requiring four and more jets. $H_{\mathrm{T}}^{\mathrm{jets}}$, for the Region 3 with $N_{b-\mathrm{jets}}$=1 (bottom, left) and Region 4 with $N_{b-\mathrm{jets}}$ ≥2 (bottom, right) selection requiring exactly three jets. All distributions are normalised to YR4 cross section of 600.8 fb.

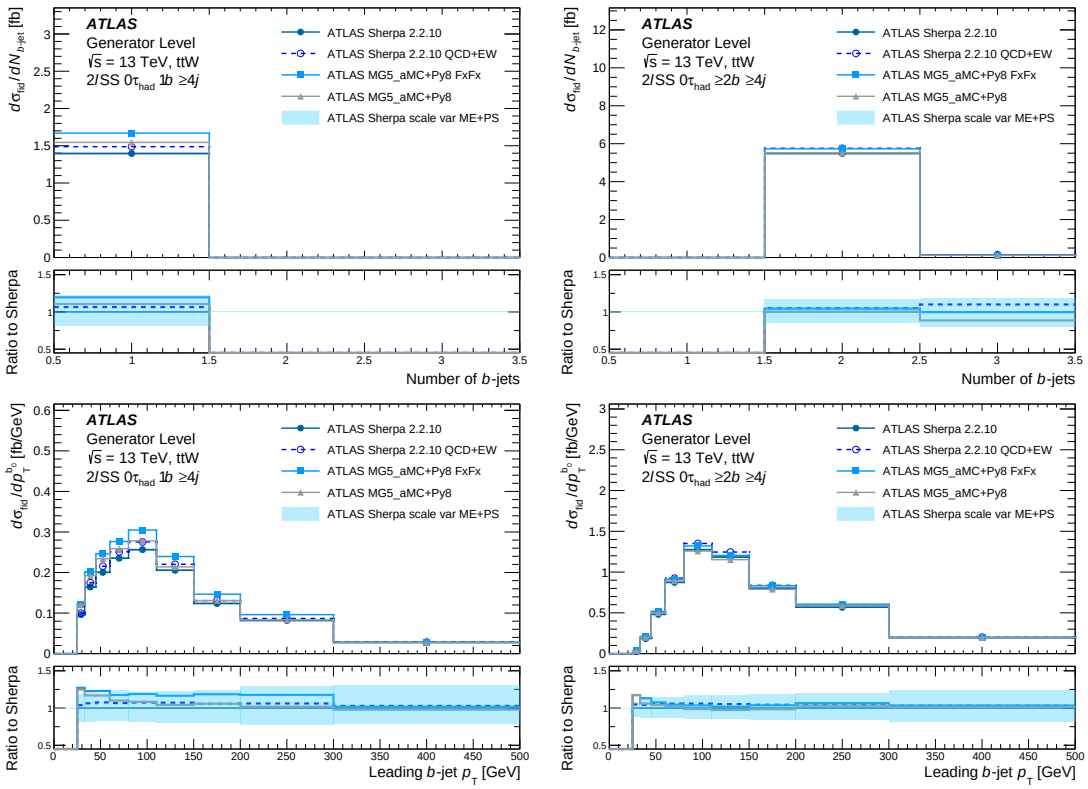

Figure 11: Distribution of the b-jet multiplicities (top) and the leading b-jet transverse momentum (bottom), for the Region 1 with $N_{b-\text{jets}}$=1 (left) and Region 2 with $N_{b-\text{jets}}$ ≥2 (right) selection requiring four and more jets. All distributions are normalised to YR4 cross section of 600.8 fb.

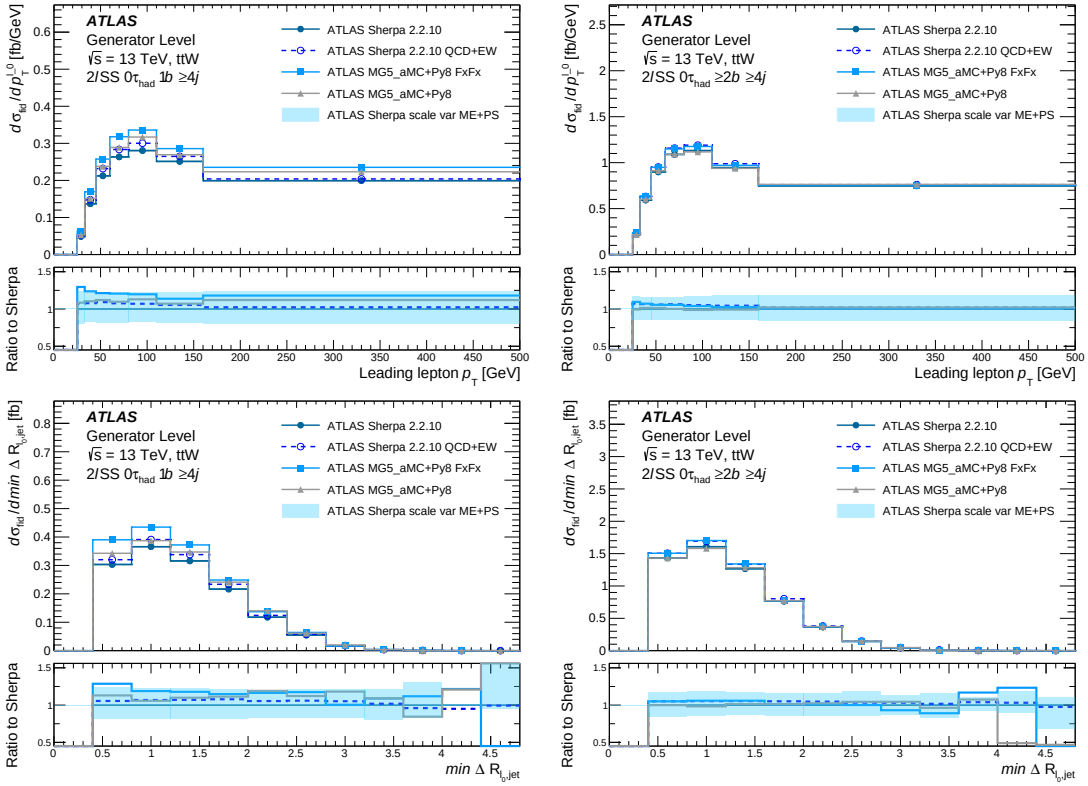

Figure 12: Distribution of the leading lepton transverse momentum (top) and the minimum angular separation between the leading lepton and the nearest jet (bottom), for the Region 1 with $N_{b-\text{jets}}$=1 (left) and Region 2 with $N_{b-\text{jets}}$ ≥2 (right) selection requiring four and more jets. All distributions are normalised to YR4 cross section of 600.8 fb.

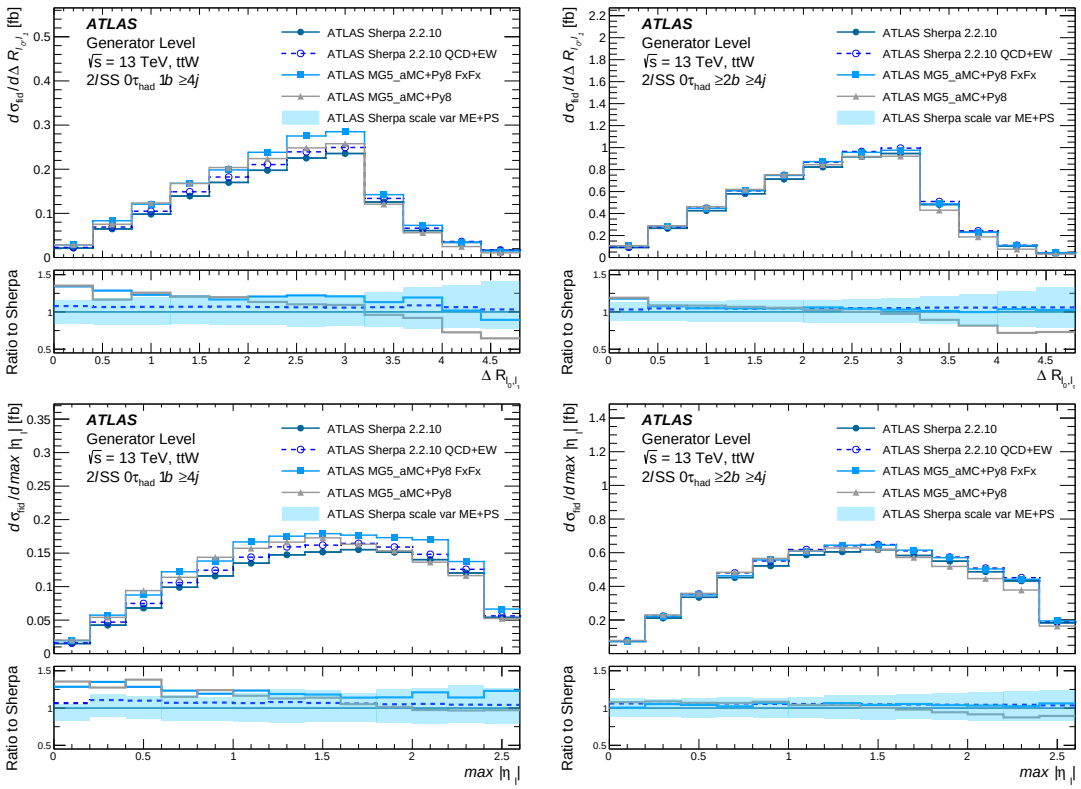

Figure 13: Distribution of the angular distance between the two leptons (top), maximum between lepton $|\eta_{\ell 0}|$ and $|\eta_{\ell 1}|$ (centre), for the Region 1 with $N_{b-\text{jets}}$=1 (left) and Region 2 with $N_{b-\text{jets}} \geq 2$ (right) selection requiring four and more jets. All distributions are normalised to YR4 cross section of 600.8 fb.

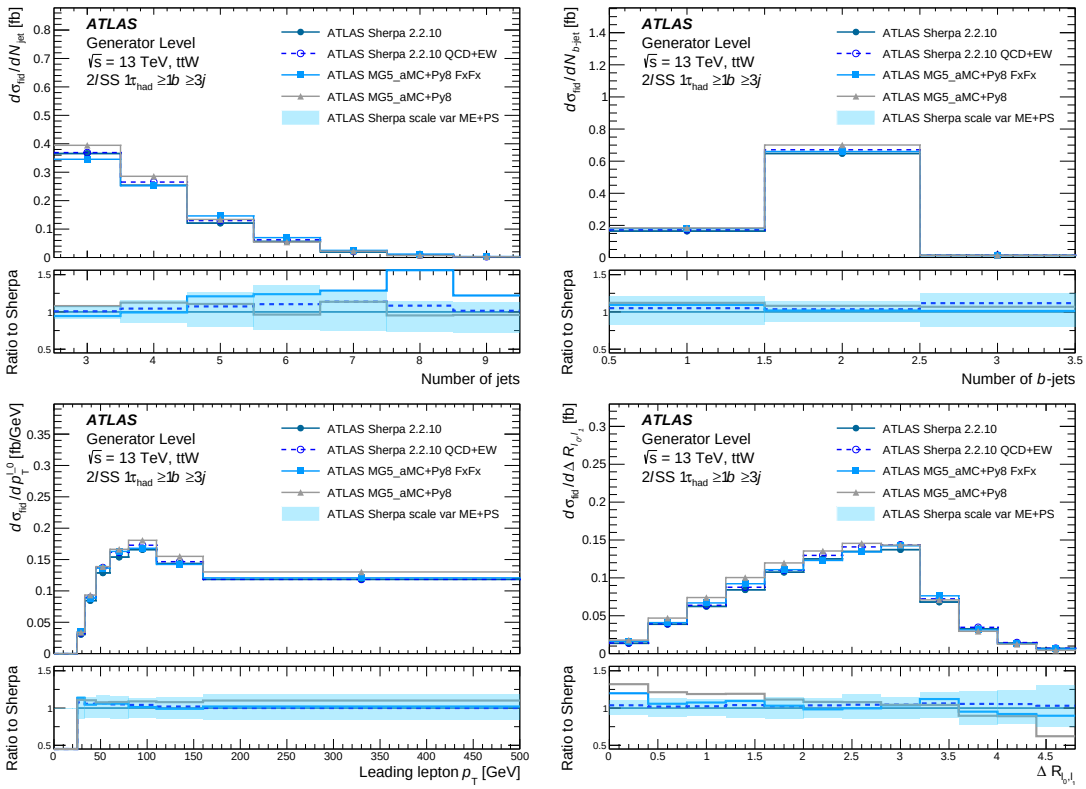

Figure 14: Distribution of the the jet multiplicity, number of b-jets, the leading lepton transverse momentum and the angular distance between the two leptons $\Delta R_{\ell\ell}$ for the Region 5 with $1\tau_{had}$ selection. All distributions are normalised to YR4 cross section of 600.8 fb.

3.4 Conclusion

The $t\bar{t}W$ preditions of SHERPA and MG5_aMC@NLO+Pythia8 with different settings have been compared in regions and observables relevant for the measurement of $t\bar{t}H$ in the multi-lepton final state. The normalised distributions sensitive to shape differences have very small scale uncertainties, below 10% in most of the phase space while these scale uncertainties are significant when the acceptance effects are included, i.e. the distributions are normalised to the $t\bar{t}W$ cross section. The inclusion of tree-level EW effects only causes minor shape effects but can lead to up to 20% difference in cross section at high jet multiplicity. As expected including the FxFx algorithm into the MG5_aMC@NLO+Pythia8 prediction leads to significant effects in all regions, especially at low H_{T}. Overall, the differences between the different model predictions are mostly within the scale uncertainty band except at the edges of the phase space. These distributions will be used as a starting point for future comparisons with CMS to derive a theory uncertainty model for a combination of the expected measurement results based on the full Run2 data set.

References

[1] ATLAS Collaboration, *Search for the standard model Higgs boson produced in association with top quarks and decaying into a $b\bar{b}$ pair in pp collisions at $\sqrt{s}$ = 13 TeV with the ATLAS detector*, Phys. Rev. D **97** (2018) 072016, arXiv: 1712.08895 [hep-ex] (cit. on pp. 2, 3, 8, 11).

[2] ATLAS Collaboration, *Measurement of Higgs boson decay into b-quarks in associated production with a top-quark pair in pp collisions at $\sqrt{s}$ = 13 TeV with the ATLAS detector*, CERN-EP-2021-202, 2021, URL: https://arxiv.org/abs/2111.06712 (cit. on pp. 2, 3).

[3] CMS Collaboration, *Measurement of* $\mathrm{t\bar{t}H}$ *production in the* $\mathrm{H} \to \mathrm{b\bar{b}}$ *decay channel in* 41.5 fb^{-1} *of proton-proton collision data at* $\sqrt{s}$ = 13 TeV, CMS-PAS-HIG-18-030, 2019, URL: https://cds.cern.ch/record/2675023 (cit. on p. 2).

[4] CMS Collaboration, *Search for* $\mathrm{t\bar{t}H}$ *production in the H*$\to \mathrm{b\bar{b}}$ *decay channel with leptonic* $\mathrm{t\bar{t}}$ *decays in proton–proton collisions at* $\sqrt{s}$ = 13 TeV, JHEP **03** (2019) 026, arXiv: 1804.03682 [hep-ex] (cit. on p. 2).

[5] ATLAS Collaboration, *Analysis of ttH and ttW production in the multilepton final states with the ATLAS detector*, ATLAS-CONF-2019-045, 2019, URL: http://cdsweb.cern.ch/record/2693930 (cit. on pp. 2, 12, 14).

[6] CMS Collaboration, *Measurement of the Higgs boson production rate in association with top quarks in final states with electrons, muons, and hadronically decaying tau leptons at* $\sqrt{s}$ = 13 TeV, Eur. Phys. J. C **81** (2021) 378, arXiv: 2011.03652 [hep-ex] (cit. on pp. 2, 12, 14).

[7] A. Bredenstein, A. Denner, S. Dittmaier and S. Pozzorini, *NLO QCD corrections to pp —> t anti-t b anti-b + X at the LHC*, Phys. Rev. Lett. **103** (2009) 012002, arXiv: 0905.0110 [hep-ph] (cit. on p. 2).

[8] M. V. Garzelli, A. Kardos and Z. Trócsányi, *Hadroproduction of $t\bar{t}b\bar{b}$ final states at LHC: predictions at NLO accuracy matched with Parton Shower*, JHEP **03** (2015) 083, arXiv: 1408.0266 [hep-ph] (cit. on p. 2).

[9] T. Ježo and P. Nason, *On the Treatment of Resonances in Next-to-Leading Order Calculations Matched to a Parton Shower*, JHEP **12** (2015) 065, arXiv: 1509.09071 [hep-ph] (cit. on pp. 2–4).

[10] T. Ježo, J. M. Lindert, N. Moretti and S. Pozzorini,
New NLOPS predictions for $t\bar{t}+b$ -jet production at the LHC, Eur. Phys. J. **C78** (2018) 502,
arXiv: 1802.00426 [hep-ph] (cit. on pp. 2, 3).

[11] T. Sjöstrand et al., *An Introduction to PYTHIA 8.2*, Comput. Phys. Commun. **191** (2015) 159,
arXiv: 1410.3012 [hep-ph] (cit. on pp. 2, 13, 15).

[12] ATLAS Collaboration, *Studies of Monte Carlo predictions for the $t\bar{t}b\bar{b}$ process*,
ATL-PHYS-PUB-2022-006 (2022), URL: https://cds.cern.ch/record/2802806
(cit. on pp. 2, 8).

[13] E. Bothmann et al., *Event Generation with Sherpa 2.2*, SciPost Phys. **7** (2019) 034,
arXiv: 1905.09127 [hep-ph] (cit. on pp. 2, 4, 12, 15).

[14] F. Cascioli, P. Maierhöfer, N. Moretti, S. Pozzorini and F. Siegert,
NLO matching for $t\bar{t}b\bar{b}$ production with massive b-quarks, Phys. Lett. **B734** (2014) 210,
arXiv: 1309.5912 [hep-ph] (cit. on pp. 2, 4).

[15] F. Cascioli, P. Maierhofer and S. Pozzorini, *Scattering Amplitudes with Open Loops*,
Phys. Rev. Lett. **108** (2012) 111601, arXiv: 1111.5206 [hep-ph] (cit. on pp. 2, 4, 12).

[16] P. Nason, *A new method for combining NLO QCD with shower Monte Carlo algorithms*,
JHEP **11** (2004) 040, arXiv: hep-ph/0409146 [hep-ph] (cit. on pp. 3, 4).

[17] S. Frixione, P. Nason and C. Oleari,
Matching NLO QCD computations with parton shower simulations: the POWHEG method,
JHEP **11** (2007) 070, arXiv: 0709.2092 [hep-ph] (cit. on pp. 3, 4).

[18] S. Alioli, P. Nason, C. Oleari and E. Re, *A general framework for implementing NLO calculations in shower Monte Carlo programs: the POWHEG BOX*, JHEP **06** (2010) 043,
arXiv: 1002.2581 [hep-ph] (cit. on pp. 3, 4).

[19] J. M. Campbell, R. K. Ellis, P. Nason and E. Re,
Top-Pair Production and Decay at NLO Matched with Parton Showers, JHEP **04** (2015) 114,
arXiv: 1412.1828 [hep-ph] (cit. on pp. 3, 4).

[20] A. Buckley et al., *Rivet user manual*, Comput. Phys. Commun. **184** (2013) 2803,
arXiv: 1003.0694 [hep-ph] (cit. on p. 3).

[21] D. J. Lange, *The EvtGen particle decay simulation package*, Nuclear Instruments and Methods in Physics Research Section A: Accelerators, Spectrometers, Detectors and Associated Equipment **462** (2001) 152, BEAUTY2000, Proceedings of the 7th Int. Conf. on B-Physics at Hadron Machines,
ISSN: 0168-9002,
URL: https://www.sciencedirect.com/science/article/pii/S0168900201000894
(cit. on p. 3).

[22] ATLAS Collaboration, *ATLAS Pythia 8 tunes to 7 TeV data*, ATL-PHYS-PUB-2014-021, 2014,
URL: https://cds.cern.ch/record/1966419 (cit. on pp. 3, 13, 15).

[23] T. Gleisberg and S. Höche, *Comix, a new matrix element generator*, JHEP **12** (2008) 039,
arXiv: 0808.3674 [hep-ph] (cit. on pp. 4, 12).

[24] S. Schumann and F. Krauss,
A Parton shower algorithm based on Catani-Seymour dipole factorisation, JHEP **03** (2008) 038,
arXiv: 0709.1027 [hep-ph] (cit. on pp. 4, 12).

[25] M. Cacciari, G. P. Salam and G. Soyez, *The anti-k_t jet clustering algorithm*, JHEP **04** (2008) 063, arXiv: 0802.1189 [hep-ex] (cit. on p. 7).

[26] M. Cacciari, G. P. Salam and G. Soyez, *FastJet user manual*, Eur. Phys. J. C **72** (2012) 1896, arXiv: 1111.6097 [hep-ph] (cit. on p. 7).

[27] M. Cacciari, G. P. Salam and G. Soyez, *The Catchment Area of Jets*, JHEP **04** (2008) 005, arXiv: 0802.1188 [hep-ph] (cit. on pp. 7, 14).

[28] CMS Collaboration, *Measurement of the cross section of top quark-antiquark pair production in association with a W boson in proton-proton collisions at $\sqrt{s}$ = 13 TeV*, CMS-PAS-TOP-21-011, 2022, URL: https://cds.cern.ch/record/2804479 (cit. on p. 12).

[29] F. Maltoni, M. L. Mangano, I. Tsinikos and M. Zaro, *Top-quark charge asymmetry and polarization in $t\bar{t}W^{\pm}$ production at the LHC*, Phys. Lett. B **736** (2014) 252, arXiv: 1406.3262 [hep-ph] (cit. on p. 12).

[30] J. M. Campbell and R. K. Ellis, *$t\bar{t}W^{+-}$ production and decay at NLO*, JHEP **07** (2012) 052, arXiv: 1204.5678 [hep-ph] (cit. on p. 12).

[31] M. V. Garzelli, A. Kardos, C. G. Papadopoulos and Z. Trocsanyi, *$t\,\bar{t}\,W^{+-}$ and $t\,\bar{t}\,Z$ Hadroproduction at NLO accuracy in QCD with Parton Shower and Hadronization effects*, JHEP **11** (2012) 056, arXiv: 1208.2665 [hep-ph] (cit. on p. 12).

[32] F. Maltoni, D. Pagani and I. Tsinikos, *Associated production of a top-quark pair with vector bosons at NLO in QCD: impact on* $t\bar{t}H$ *searches at the LHC*, JHEP **02** (2016) 113, arXiv: 1507.05640 [hep-ph] (cit. on p. 12).

[33] F. Febres Cordero, M. Kraus and L. Reina, *Top-quark pair production in association with a $W^{\pm}$ gauge boson in the POWHEG-BOX*, Phys. Rev. D **103** (2021) 094014, arXiv: 2101.11808 [hep-ph] (cit. on p. 12).

[34] S. Frixione, V. Hirschi, D. Pagani, H. .-S. Shao and M. Zaro, *Electroweak and QCD corrections to top-pair hadroproduction in association with heavy bosons*, JHEP **06** (2015) 184, arXiv: 1504.03446 [hep-ph] (cit. on p. 12).

[35] D. de Florian et al., *Handbook of LHC Higgs Cross Sections: 4. Deciphering the Nature of the Higgs Sector*, 2017, arXiv: 1610.07922 [hep-ph] (cit. on pp. 12, 23).

[36] J. Alwall et al., *The automated computation of tree-level and next-to-leading order differential cross sections, and their matching to parton shower simulations*, JHEP **07** (2014) 079, arXiv: 1405.0301 [hep-ph] (cit. on p. 12).

[37] S. von Buddenbrock, R. Ruiz and B. Mellado, *Anatomy of inclusive $t\bar{t}W$ production at hadron colliders*, Phys. Lett. B **811** (2020) 135964, arXiv: 2009.00032 [hep-ph] (cit. on p. 12).

[38] R. Frederix and I. Tsinikos, *On improving NLO merging for* $t\bar{t}W$ *production*, JHEP **11** (2021) 029, arXiv: 2108.07826 [hep-ph] (cit. on p. 12).

[39] J. A. Dror, M. Farina, E. Salvioni and J. Serra, *Strong tW Scattering at the LHC*, JHEP **01** (2016) 071, arXiv: 1511.03674 [hep-ph] (cit. on p. 12).

[40] R. Frederix, D. Pagani and M. Zaro, *Large NLO corrections in $t\bar{t}W^{\pm}$ and $t\bar{t}t\bar{t}$ hadroproduction from supposedly subleading EW contributions*, JHEP **02** (2018) 031, arXiv: 1711.02116 [hep-ph] (cit. on pp. 12, 13).

[41] A. Kulesza, L. Motyka, D. Schwartländer, T. Stebel and V. Theeuwes, *Associated production of a top quark pair with a heavy electroweak gauge boson at NLO+NNLL accuracy*, Eur. Phys. J. C **79** (2019) 249, arXiv: 1812.08622 [hep-ph] (cit. on p. 12).

[42] A. Broggio et al., *Top-quark pair hadroproduction in association with a heavy boson at NLO+NNLL including EW corrections*, JHEP **08** (2019) 039, arXiv: 1907.04343 [hep-ph] (cit. on p. 12).

[43] A. Kulesza, L. Motyka, D. Schwartländer, T. Stebel and V. Theeuwes, *Associated top quark pair production with a heavy boson: differential cross sections at NLO+NNLL accuracy*, Eur. Phys. J. C **80** (2020) 428, arXiv: 2001.03031 [hep-ph] (cit. on p. 12).

[44] G. Bevilacqua, H.-Y. Bi, H. B. Hartanto, M. Kraus and M. Worek, *The simplest of them all: $t\bar{t}W^{\pm}$ at NLO accuracy in QCD*, JHEP **08** (2020) 043, arXiv: 2005.09427 [hep-ph] (cit. on p. 12).

[45] A. Denner and G. Pelliccioli, *NLO QCD corrections to off-shell $t\bar{t}W^{+}$ production at the LHC*, JHEP **11** (2020) 069, arXiv: 2007.12089 [hep-ph] (cit. on p. 12).

[46] G. Bevilacqua et al., *NLO QCD corrections to off-shell $t\bar{t}W^{\pm}$ production at the LHC: correlations and asymmetries*, Eur. Phys. J. C **81** (2021) 675, arXiv: 2012.01363 [hep-ph] (cit. on p. 12).

[47] A. Denner and G. Pelliccioli, *Combined NLO EW and QCD corrections to off-shell $t\bar{t}W$ production at the LHC*, Eur. Phys. J. C **81** (2021) 354, arXiv: 2102.03246 [hep-ph] (cit. on p. 12).

[48] G. Bevilacqua et al., *Modeling uncertainties of $t\bar{t}W^{\pm}$ multilepton signatures*, Phys. Rev. D **105** (2022) 014018, arXiv: 2109.15181 [hep-ph] (cit. on p. 12).

[49] T. Gleisberg et al., *Event generation with SHERPA 1.1*, JHEP **02** (2009) 007, arXiv: 0811.4622 [hep-ph] (cit. on p. 12).

[50] S. Hoeche, F. Krauss, M. Schonherr and F. Siegert, *QCD matrix elements + parton showers: The NLO case*, JHEP **04** (2013) 027, arXiv: 1207.5030 [hep-ph] (cit. on pp. 12, 15).

[51] J. Alwall et al., *The automated computation of tree-level and next-to-leading order differential cross sections, and their matching to parton shower simulations*, Journal of High Energy Physics **2014** (2014), URL: https://doi.org/10.1007%2Fjhep07%282014%29079 (cit. on pp. 13, 15).

[52] R. Frederix and S. Frixione, *Merging meets matching in MC@NLO*, JHEP **12** (2012) 061, arXiv: 1209.6215 [hep-ph] (cit. on pp. 13, 15).

[53] ATLAS Collaboration, *Modelling of rare top quark processes at $\sqrt{(s)}$=13TeV*, ATL-PHYS-PUB-2020-024 (2020), URL: http://cdsweb.cern.ch/record/2730584 (cit. on p. 13).

[54] J. Alwall et al., *A Standard format for Les Houches event files*, Comput. Phys. Commun. **176** (2007) 300, arXiv: hep-ph/0609017 [hep-ph] (cit. on p. 15).

[55] R. D. Ball et al., *Parton distributions for the LHC Run II*, JHEP **04** (2015) 040, arXiv: 1410.8849 [hep-ph] (cit. on p. 15).